Mine Closure 2026 – AB Fourie, G Boggs, J Heyes & M Tibbett (eds)

doi:10.36487/ACG_repo/2615_85

Sequential extraction to assess metal retention and mobility in acid mine drainage-impacted sediments from the Witkranz legacy mine, South Africa

Mafeto Malatji [a,c,*], Tebogo Makono [a], Khomotso Sekiba [a], Viswanath Vadapalli [a,c], Godfrey Madzivire [a], Elvis Fosso-Kankeu [b], Edward Malenga [b]

[a] *Minerals, Energy, Environment and Groundwater Unit, Council for Geoscience, South Africa*

[b] *Department of Metallurgy, University of Johannesburg, South Africa*

[c] *Department of Geology, University of Free State, South Africa*

Abstract

A sequential extraction procedure was conducted to evaluate metal retention and mobility in sediments collected along the channel transporting acid mine drainage (AMD) from the Witkranz legacy mine discharge point into the Boesmanspruit stream in Carolina, Mpumalanga, South Africa. The AMD is characterised by low pH (3.1) and elevated metal (22 mg/L Fe and 30 mg/L Mn) and sulphate concentrations (1098 mg/L). Contaminated waters ultimately flow through the Boesmanspruit stream into the Boesmanspruit and Nooitgedacht dams, posing risks to downstream ecosystems, human health and aquatic life.

Sequential extraction evaluates the physico-chemical forms of mobile metals rather than their concentration, hence its use in this study. The results indicated that Mn is mostly associated with the exchangeable fraction, making it highly mobile in the area. Fe is associated with both the exchangeable and reducible fractions, giving it moderate mobility. Ca is mainly associated with the residual fraction but can become available due to its significant association with the exchangeable fraction (42%). Cr is largely associated with the reducible fraction, remaining stable under oxidising conditions; however, it can become mobile under reducing conditions. Mg is mostly associated with F3 and the residual fractions, remaining stable and immobile. The general order of mobility is Mn > Fe > Ca > Cr > Mg.

Overall, these findings show that the sediments are not only a sink for metals but also a potential long-term secondary source of contamination under changing physico-chemical conditions.

Keywords*: contaminated water, elevated metals, sulphate concentrations, physico-chemical conditions*

1 Introduction

Acid mine drainage (AMD) contamination in rivers is a global environmental concern driven by mining activities and improper waste disposal (Zhou et al. 2020; Aswal et al. 2023; Lloyd 2013; Shongwe 2018). AMD is generated through the oxidation of sulphide-bearing minerals in the presence of water, producing an acidic solution (Munnik 2010; McCarthy 2011). The process is catalysed by Thiobacillus bacteria, and the resultant solution is typically characterised by low pH (< 4.5), high salinity, and elevated concentrations of sulphate, metals and metalloids (Sakala et al. 2017; Ojonimi et al. 2019). Such characteristics exacerbate the toxicity of AMD in receiving environments, thereby enhancing metal solubility, mobility and bioavailability (Sakala et al. 2017; Miller et al. 2019). According to Malatji (2025), AMD causes environmental damage and changes that can be difficult to manage in the long term: one being that AMD precipitates ferric hydroxide in aquatic environments, resulting in low dissolved oxygen that leads to asphyxiation in receiving environments (CSIR 2013; Jennings 2008). Moreover, elevated concentrations of metals become bioavailable and mobile, which

* Corresponding author. Email: rmalatji@geoscience.org.za

can lead to the pollution of surface and groundwater, poor soil quality, and poor health of aquatic flora and fauna (Ojonimi et al. 2019).

Metal mobility depends more on the metal's physico-chemical forms than on total concentration (Violante et al. 2010; Landner & Reuther 2005; Favas et al. 2011). The geochemical partitioning of metals between different environmental phases, primarily the water column and sediments, is driven by physico-chemical and environmental factors such as changes in pH and redox, as well as the composition of sediments (Korfali & Davies 2004; Tessier et al. 1979; Galán et al. 2003). Upon entering aquatic systems, metals may occur as: (1) dissolved forms, which are freely hydrated ions that are readily available for biological uptake; (2) sorbed forms where metals are adsorbed onto suspended particles or sediment surfaces and often complexed with clay minerals or organic matter; and (3) bound forms strongly associated with sediments that have limited mobility (Miranda et al. 2022; Tessier et al. 1979; Namiesnik & Rabajczyk 2010; Galán et al. 2003). Furthermore, metals associated with sediments may be partitioned into specific geochemical fractions such as exchangeable, reducible, oxidisable and residual fractions (Manyatshe 2017; Galán et al. 2003).

Although the elemental concentrations of metals in the sediments have been quantified, their physico-chemical forms, which govern metal mobility, have not yet been evaluated, especially under the influence of AMD in the study area; thus they present a research gap. Determining the geochemical partitioning of metals is essential for understanding their behaviour, interactions within sediments and potential environmental risks. Sequential extraction is a speciation method that is commonly applied to evaluate geochemical partitioning of metals in soils and sediments. In this study, a 4-stage sequential extraction procedure based on the European Standard, Measurements and Testing (SM&T) program, as adopted by Nemati et al. (2011) and Tokalioglu et al. (2003), was employed. Each step of this method uses specific reagents to sequentially separate metals associated with different geochemical fractions.

- Exchangeable fraction (carbonate bound): This fraction consists of metals weakly bound to sediment or soil particles that can be released through ion exchange processes or slight decreases in pH, making them highly mobile. Acidic AMD conditions can induce such ion exchanges through the dissolution of carbonate minerals, thereby reducing their buffering capacity. As a result, this fraction poses the greatest immediate environmental risk.
- Reducible fraction (bound to Fe and Mn oxides): Metals in this fraction are bound to iron and manganese oxides and can be released under unstable reducing conditions. Fe and Mn are produced as secondary minerals during AMD attenuation under reducing conditions, which leads to temporary immobilisation. This fraction is therefore considered moderately mobile.
- Oxidisable fraction (bound to organic matter and sulphides): Metals are associated with organic matter and sulphide minerals in this fraction, and are generally stable under reducing conditions, but may be released under oxidising conditions that AMD can produce. Depending on redox fluctuations, their mobility can be high.
- Residual fraction: Metals in this fraction are structurally bound with the crystalline structure of minerals and can only be released under extreme conditions that AMD is incapable of producing. Therefore, they are considered immobile under natural environmental conditions (Benamer 2014; Singh et al. 2005; Tessier et al. 1979).

Based on the different geochemical fractions established, this study aims to investigate the retention and distribution of metals in sediments along the channel through which AMD flows from the Witkranz legacy mine discharge point into the Boesmanspruit stream.

To achieve this, the following objectives were devised:

- Evaluate the dispersion of selected metals across different geochemical fractions in the sediments using a modified SM&T sequential extraction procedure, thereby identifying their behaviour and environmental risks under the prevailing geochemical conditions.

- Characterise sediment mineralogy and elemental composition using X-ray diffraction (XRD) and X-ray fluorescence (XRF) to identify secondary mineral precipitation.
- Assess the quality of the water along the study area for comparison with sediment results.

1.1 Study area

The Witkranz discharge point is situated on Portion 11 of the Witkranz 53 IT Farm, approximately 10 km south of Carolina in Mpumalanga province. The site falls within the quaternary drainage region X11B, part of the Komati West subcatchment in the Inkomati Water Management Area (Figure 1) (Novhe et al. 2016; Chidzungu 2019). The Witkranz discharge point is one of several acidic mine water outflows entering the Boesmanspruit stream, which flows north-westerly into the Boesmanspruit dam, Carolina's primary freshwater supply. Water discharged at this point is highly acidic (pH 3.1) with elevated electrical conductivity and high concentrations of contaminants, including Fe (22 mg/L), Mn (30 mg/L) and SO_4^{2-} (1098 mg/L). Previous studies (Mello et al. 2024; Dube et al. 2019; Mashalane et al. 2018; Novhe et al. 2016) have documented AMD generation and its environmental impacts in the area, including metal contamination in the receiving stream. The water originates from a spring that is presumed to decant from old underground mine workings (Mello et al. 2024). The discharge flows into the Boesmanspruit stream, which also lies within the X11B quaternary catchment in the upper Komati catchment. The stream feeds into both the Boesmanspruit and Nooitgedacht dams before ultimately joining the Komati River. The Komati River forms part of the international boundary between South Africa, Eswatini and Mozambique (Dzhangi & Atangana 2024; McCarthy & Humphries 2013; Nethavhani 2012).

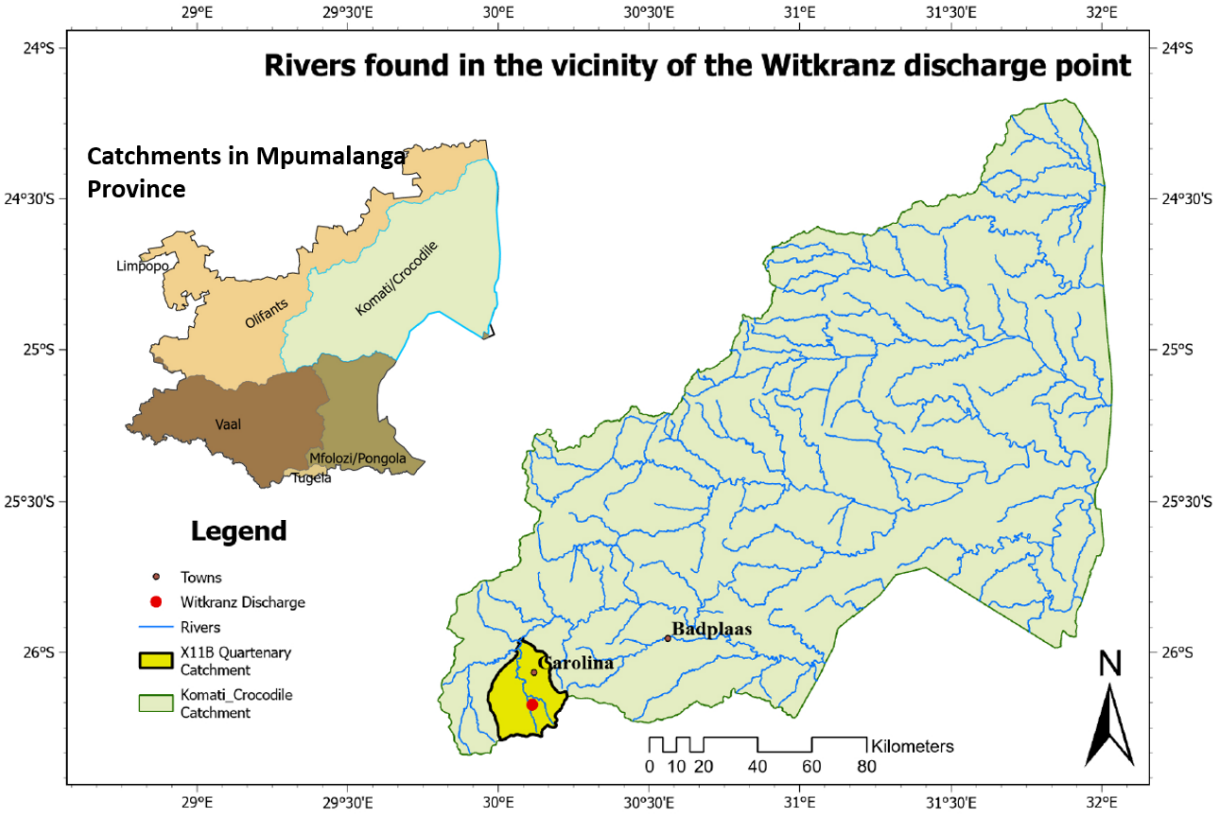

Figure 1 Map showing rivers found in the vicinity of the Witkranz discharge point and the location X11B quaternary catchment in the Inkomati Crocodile catchment

The area is located within the eastern Highveld of South Africa and receives a mean annual rainfall of approximately 808.5 mm, with most precipitation occurring during the summer months. Land use in the area is mixed and includes mining, agriculture (livestock and crop farming) and game farming (Chidzungu 2019). Geologically, the study area lies within the Ermelo Coalfield, the coal seams of which occur within the Vryheid

Formation of the Ecca Group, which forms part of the Karoo Supergroup. Lithologically, the coal seams are interbedded with fine to coarse grained sandstones, siltstones and mudstones. Mineralogically, the coal seams consist primarily of sulphate-producing minerals such as pyrite and quartz (Greenshields 1986; Geldenhuis & Bell 1998; Hancox & Götz 2014). The pyrite, a typical sulphide mineral, undergoes oxidation in the presence of water to produce an acidic leachate referred to as AMD. This results in an increased concentration of metals and SO_4 and low pH in affected aquatic environments (Munnik, 2010; McCarthy 2011). Other minerals present in the study area include clay minerals (kaolinite and illite) and carbonates (calcite, dolomite, ankerite and siderite), which act as buffering minerals (Greenshields 1986; Geldenhuis & Bell 1998; Hancox & Götz 2014). A typical carbonate mineral, such as calcite, counteracts AMD by dissolving into solution, thereby buffering the pH (Pope et al. 2010).

2 Methodology

2.1 Sampling

To investigate the contamination, a sampling path following the downward flow of water covering an area of approximately 2 km was set up (Table 1 and Figure 2). To evaluate the evolution of the contamination, a total of 6 sediment samples were collected along the flow path. The sampling points were spatially selected to include:

- One sampling point before the discharge point, representing the baseline before mixing with AMD
- 2 points along the flow path, downstream of the discharge point, representing the travel and settling of contaminants along the flow path
- one point at the confluence with the Boesmanspruit stream, to represent the entry of the contaminants into the river system
- 2 points further downstream within the Boesmanspruit stream, to represent the long-term settling into the stream.

Sediment samples were collected during the wet season using the grab sampling method. Sampling was conducted along the banks of the channel, and the upper 5 cm of sediment was collected to represent the most reactive material. Approximately 4–5 kg of composite sediment samples was collected at an estimated area of $1m^2$ per site to ensure sufficient volumetric, spatial representation as well as reproducibility. The samples were placed in plastic bags and immediately sealed to minimise oxidation, then transported to the lab for the sequential extraction procedure as well as mineralogical and chemical analyses.

Six water samples to coincide with the sediment samples were also collected at each sampling point using 100 mL high-density polyethylene (HDPE) bottles; the flow rate was measured at an average of 34 L/s. In situ measurements of pH, electrical conductivity (EC), redox potential (Eh), dissolved oxygen (DO), temperature, and total dissolved solids were conducted using a Hach HQ40d portable multimeter. The samples were filtered using 0.45 µm membrane filters to separate dissolved constituents from suspended particulates. Samples for metal analysis were acidified by adding 3–5 drops of 3 M nitric acid. All collected samples were stored at approximately 4 °C before metal and non-metal analysis.

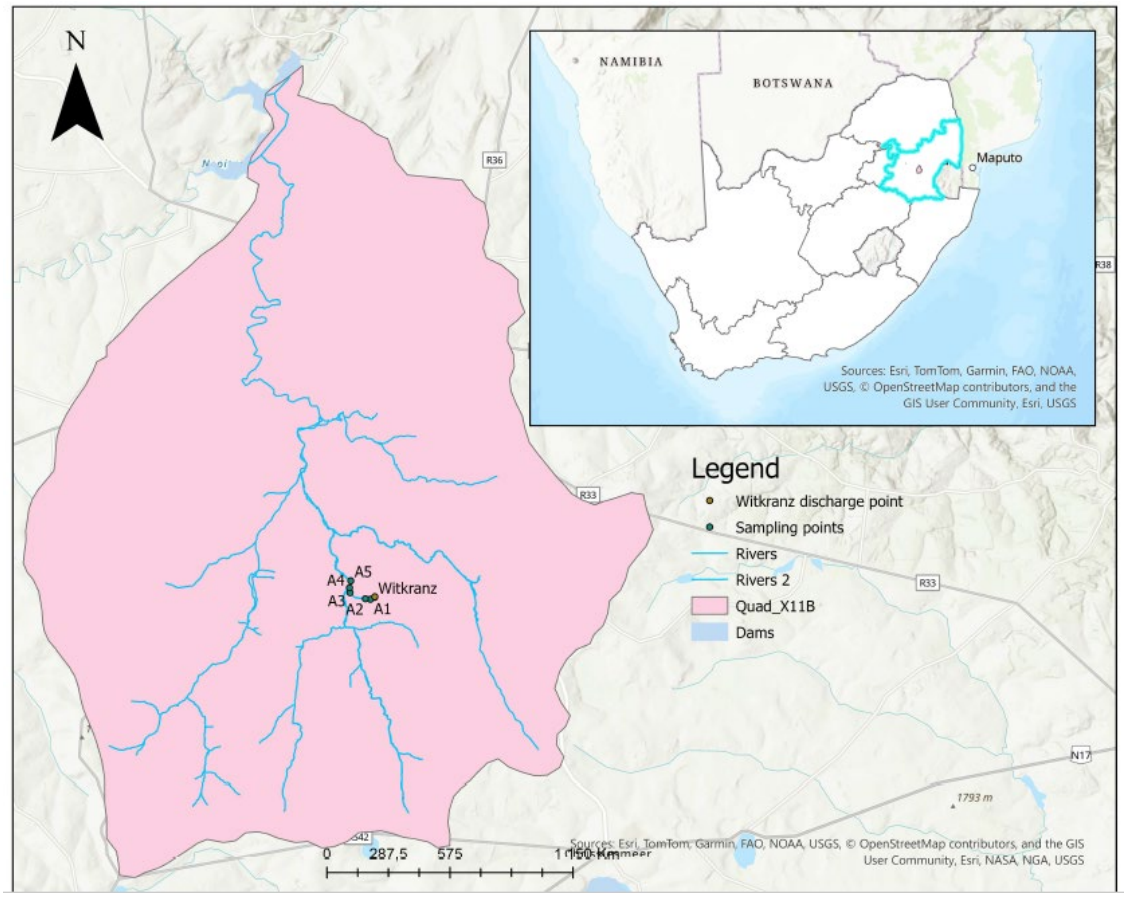

Figure 2 Map showing sampling points in the study area

Table 1 Description of sampling points

Sample number	Description	Coordinates	
B1	Seepage point before the discharge point (upstream)	-26.1736945	30.1126473
A1	Point after the discharge point	-26.1745322	30.1108663
A2	Point before the discharge point (downstream)	-26.1743397	30.1088278
A3	Point just before the confluence with the Boemanspruit	-26.1717155	30.1023956
A4	Boemanspruit downstream point 1	-26.1696964	30.1021448
A5	Boemanspruit downstream point 2	-26.1667659	30.1026883

2.2 Characterisation of sediments by X-ray fluorescence and X-ray diffraction

2.2.1 X-ray fluorescence sample preparation and analysis

The sediment samples were milled (< 75 µ fraction) and first dried for at least 3 hours at 100 °C, and then roasted at 1,000 °C for at least 3 hours to oxidise Fe^{2+} and S, which are detrimental to the Pt ware used to prepare glass disks. The loss of ignition (LOI) and moisture (H_2O^-) is determined gravimetrically during the drying and roasting steps. The glass disks were prepared by fusing 1 g of the roasted sample and 10 g of flux consisting of 49.50% $Li_2B_4O_7$, 49.50 $LiBO_2$ and 1.00% LiBr at 950 °C. The glass disks were then analysed by a

PANalytical Axios XRF spectrometer equipped with a 4 kW Rh tube. For trace element analysis, a 12 g milled sample and 3 g of Licowax were mixed and pressed into a powder briquette by a hydraulic press with the applied pressure at 25 tonnes. The pressed powder pellets were analysed for the trace elements by a PANalytical Zetium XRF spectrometer also equipped with a 4 kW Rh tube (Cloet 2022).

2.2.2 X-ray diffraction sample preparation and analysis

Instrumentation and measurement conditions: XRD measurements are performed on a Bruker D8 ADVANCE instrument with 2.2kW Cu long, fine focus tube (Cu Kα, λ=1.54060) and a 90-position sample changer. The system is equipped with a LynxEye detector with a 3.7º active area. Samples are scanned from 2 to 70° 2θ at a speed of 0.02° 2θ steps size/0.5 sec, and generator settings of 40 kV and 40mA.

2.2.2.1 Sample processing

For bulk (whole rock) analysis, a representative sample of the rock or soil material is crushed and milled to a fine powder of around 20 μm in size. A subsample is pressed into a shallow plastic sample holder against a rough filter paper in order to ensure random orientation.

2.2.2.2 Data processing and analysis

Phase identification is based on the Bruker DIFFRAC^{Plus} EVA evaluation program. Routinely, phase concentrations are determined as semi-quantitative estimates (with accuracy ±5%) using the reference intensity ratio method and relative peak heights/areas proportions (Brime 1985).

2.3 Characterisation of water samples

For the water samples, ion chromatography (IC) was employed to determine the concentrations of major anions (e.g. SO_4^{2-}, NO_3^-, Cl^-). Inductively coupled plasma mass spectrometry (ICP-MS) was used to quantify metal concentrations. The calibration and analytical procedures are detailed below.

2.3.1 Ion chromatography

2.3.1.1 Calibration procedure

Prior to sample analysis, the IC instrument is calibrated using certified reference standards prepared at appropriate concentration levels covering the expected analytical range. Calibration standards are prepared from traceable stock solutions in accordance with the laboratory's standard preparation procedures.

A calibration blank and a minimum of 5 calibration standards are analysed to establish the calibration curve. The calibration must meet the laboratory's acceptance criteria, including the required correlation coefficient (R^2) of not less than the laboratory-defined acceptance limit (typically ≥ 0.995). Calibration verification standards are analysed after calibration and periodically throughout the analytical batch to verify instrument stability. Calibration is repeated whenever the acceptance criteria are not met or after instrument maintenance.

2.3.1.2 Analysis procedure

Samples are received, logged and prepared according to the applicable sample preparation procedure. and are filtered before analysis. The IC system operates under the validated chromatographic conditions specified in the analytical method, including:

- eluent composition and flow rate
- column type and temperature
- injection volume
- suppressor operating conditions

- detector settings.

Each analytical batch includes a:

- method blank
- calibration verification standard
- laboratory control sample
- duplicate sample.

Peak identification is based on retention time comparison with calibration standards, while quantification is performed using the approved calibration curve. Analytical quality control results are reviewed before reporting results. Samples failing quality control acceptance criteria are investigated and, where appropriate, reanalysed.

2.3.2 Inductively coupled plasma mass spectrometry

2.3.2.1 Calibration procedure

The ICP-MS instrument is calibrated using multi-element certified reference standards prepared from traceable stock solutions covering the required analytical concentration range. Internal standards are added to all calibration standards, blanks, quality control samples and test samples to correct for instrumental drift and matrix effects. A calibration blank and multiple calibration standards are analysed to generate the calibration curve. The calibration must comply with the laboratory's acceptance criteria for linearity, calibration residuals and response stability. Initial calibration verification (ICV) and continuing calibration verification (CCV) standards are analysed at defined intervals to confirm calibration validity throughout the analytical sequence. Instrument performance checks, including mass calibration, detector optimisation and sensitivity, are performed before sample analysis in accordance with the manufacturer's recommendations.

2.3.2.2 Analysis procedure

Samples are filtered, digested, diluted or otherwise prepared in accordance with the applicable analytical method prior to analysis. The ICP-MS instrument is operated using validated operating conditions, including:

- plasma power
- nebuliser gas flow
- auxiliary gas flow
- sample uptake rate.

Each analytical batch includes a/n:

- method blank
- calibration blank
- ICV
- CCV
- duplicate sample
- certified reference material.

Quantification is performed using the established calibration curve with internal standard correction applied. Instrument drift is monitored throughout the analytical sequence using CCV standards and internal standard recoveries. Samples exceeding the calibration range are diluted and reanalysed. Analytical results are only reported after all quality control samples have met the specified acceptance criteria.

2.3.2.3 Quality assurance

For both IC and ICP-MS analyses:

- Only calibrated and verified equipment is used.
- Certified reference materials and traceable standards are used for calibration.
- Instrument maintenance is performed according to the manufacturer's recommendations and laboratory maintenance schedules.
- Calibration, quality control, maintenance and analytical records are retained in accordance with the laboratory's document control and record retention procedures.
- All analytical activities are performed by trained and authorised personnel following the requirements of ISO/IEC 17025.

2.4 Standard, Measurements and Testing extraction protocol (sequential extraction method)

The SM&T extraction procedure was applied to fractionate metals in the sediment samples. This method enables the partitioning of metals into operationally defined fractions (exchangeable, reducible, oxidisable and residual), thereby providing insight into their mobility, bioavailability and potential environmental risk. This method involves 4 main steps, each targeting different metal fractions (see Figure 3):

Step 1 – exchangeable fraction

40mL of 0.11 M acetic acid was added to 1g of dry sediment sample (1:20 w/v ratio). The mixture was shaken at a speed of 250 rpm for 16 hours at 22 °C. The extract was separated from the solid phase by centrifugation at 3,800 rpm for 20 minutes. The supernatant liquid was decanted into a 50 mL polypropylene centrifuge tube and stored in a refrigerator at 4°C before analysis. The residue was washed by adding 20 mL of double-distilled water, shaken for 15 minutes and then centrifuged again for 20 minutes at 3,800 rpm. The second supernatant liquid was discarded to avoid any loss of residue.

Step 2 – Reducible fraction

Metals bound to iron and manganese oxides were extracted by adding 40 mL of 0.1 M hydroxyl ammonium chloride (NHOH HCl) (adjusted to pH 2 with 2 M nitric acid) onto the residue from the first step (1:4 w/v ratio). After shaking the mixture for 16 hours at 22 °C at a speed of 250 rpm, it was centrifuged for 15 minutes and then decanted as described in step 1. The residue was washed by adding 20 mL of distilled water, centrifuged and then the supernatant was discarded as described in step 1 before proceeding to the next step.

Step 3 – Oxidisable fraction

10 mL of 8.8 M hydrogen peroxide (pH of 2_3) was carefully added in small aliquots to the residue in the centrifuge tube. The tube was covered loosely (to prevent substantial loss of H_2O_2) and the residue was digested at room temperature for 1 hour with occasional shaking (1:2 w/v digest ratio). The content in the tube was continuously digested for 1 hour at 85°C in a water bath, with occasional shaking for the first 30 minutes, and the volume was reduced to 2–3 mL by further heating the uncovered tube. An additional 10 mL of H_2O_2 (pH of 2-3) was added to the tube and the covered tube was heated to 85°C and digested for 1 hour before the volume in the uncovered tube was reduced to dryness. After cooling, 50 mL of 1.0 M ammonium acetate (adjusted to pH 2 by adding concentrated HNO_3) was added to the residue and the mixture was shaken for 16 hours at 22°C at 250 rpm (1:5 w/v extraction ratio). The extract was separated from the solid phase by centrifugation and decantation as previously described and stored at 4°C.

Step 4 – Residual fraction

The residue from the third step was digested using aqua regia (HNO_3 + 3HCl) for metals insoluble in the previous steps. For this purpose, first 6 mL of distilled water and then the aqua regia solution in a sequence of 15 and 10 mL were introduced into the same residue. After adding each aqua regia solution, the residue was evaporated to near dryness in a water bath (1:3.1 w/v aqua regia ratio). The extract was filtered through

filter paper by adding 1 M HNO_3 solution in small amounts on the last residue in the centrifuge tube (Nemati et al. 2011; Tokalioglu et al. 2003).

The sequential extraction procedure was carried out at the Extractive Metallurgy Laboratory, Doornfontein Campus, University of Johannesburg. The university supplied all analytical-grade reagents and deionised water used during sample preparation and analysis. Working solutions were prepared by diluting concentrated stock solutions with distilled water to the required molarities. Where required, pH adjustments were performed.

The residual sediments were subsequently analysed using XRD and XRF to determine their mineralogical and elemental composition following the extraction procedure.

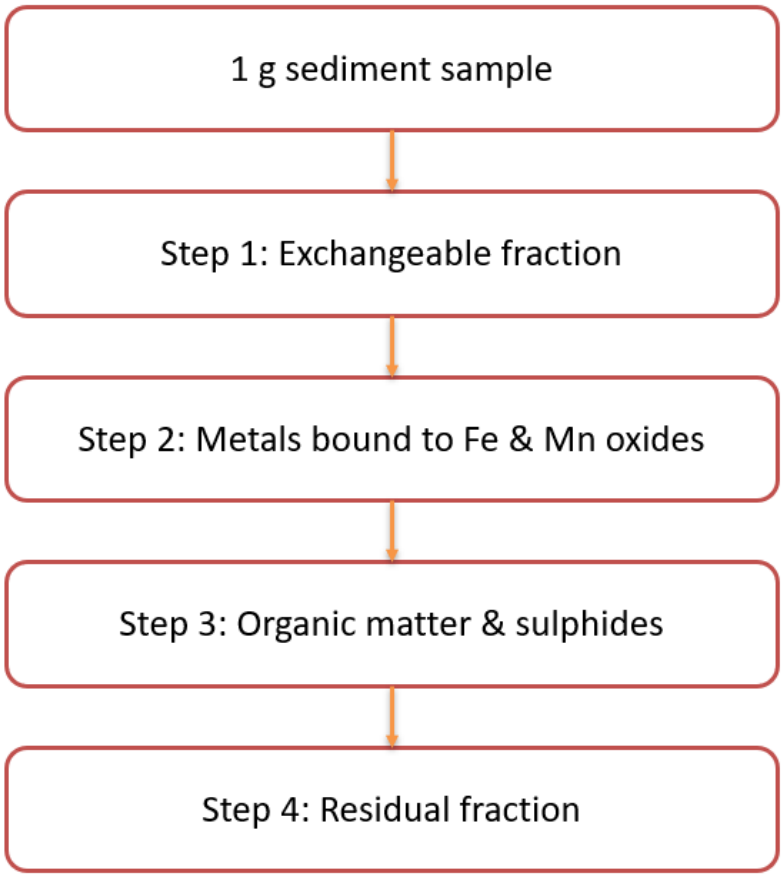

Figure 3 Flow diagram of the Standard, Measurements and Testing extraction procedure

3 Results and discussion

3.1 Baseline elemental and mineralogical composition

The elemental analysis indicated that the sediments were predominantly composed of SiO_2, ranging between 63.63 and 91.20% in all samples. Al_2O_3 was the second most abundant oxide, ranging between 3.95 and 13.01%. The concentration for Fe_2O_3 ranged between 1.22 and 5.15%, followed by K_2O ranging from 0.78 and 2.07. The concentration for other oxides was low; these included TiO_2, MnO, MgO, CaO, Na_2O, P_2O_5 and Cr_2O_3 (see Table 2).

Table 2 Baseline elemental composition

	A1	A2	A3	A4	A5	B1
SiO_2	63.63	82.88	80.16	73.89	91.20	81.54
TiO_2	0.537	0.374	0.64	0.76	0.25	0.423
Al_2O_3	13.01	7.03	7.25	11.57	3.95	6.21
Fe_2O_3 (t)	1.80	1.22	2.14	2.31	1.49	5.15
MnO	0.018	0.010	0.020	0.051	0.011	0.021
MgO	0.13	<0.02	<0.02	0.09	<0.02	0.20
CaO	0.09	0.05	0.06	0.13	0.04	0.05
Na_2O	0.04	<0.02	<0.02	0.13	0.07	<0.02
K_2O	1.42	0.83	1.08	2.07	1.47	0.78
P_2O_5	0.080	0.050	0.070	0.110	0.030	0.060
Cr_2O_3	0.018	0.010	0.020	0.020	0.011	0.106
LOI	19.17	7.60	8.69	8.79	1.41	5.33
Total	99.94	100.09	100.17	99.92	99.95	99.89
H_2O^-	5.52	2.79	3.88	4.60	0.74	1.15

The mineralogical analysis indicated that the sediments were predominantly composed of quartz; other minerals observed included K-feldspar and clinochlore. The mineralogy showed variations from point to point, with quartz being the dominant mineral across sampling points B1 to A5. K-feldspar was only recorded at A4 and A5, with a sole clinochlore at A1 (see Table 3). The composition of the sediments is mostly siliceous, reflecting the dominance of quartz, which has a poor metal adsorption capacity. This can influence the retention of metals in the sediments.

Table 3 Baseline mineralogical composition

Sample ID	K-feldspar	Quartz	Clinochlore
B1	–	100	–
A1	–	68	32
A2	–	100	–
A3	–	100	–
A4	10	90	–
A5	8	92	–

3.2 Water quality

The physico-chemical parameters and metal concentrations measured in the study area are summarised in Tables 4 and 5. In terms of in situ parameters, it was observed that most sampling points exceeded the acceptable limits (South African Bureau of Standards 2022) and exhibited acidic conditions (pH < 5), except B1, A4 and A5. The relatively higher pH at B1 (> 4) reflects upstream conditions prior to AMD mixing. A pronounced decrease in pH from A1 to A3 confirms the strong geochemical influence of AMD inflow, which results in the oxidation of pyrite, releasing acidity and elevated SO_4 and metals; thereby resulting in the decrease in pH. Acidic conditions enhance metal solubility and mobility as metals predominantly occur as

soluble cations at low pH (< 5) (Mitra et al. 2022; Maphanga et al. 2024). Downstream at A4 and A5, pH partially recovers; likely due to the combined effects of dilution and the buffering capacity of carbonate minerals, which form part of the geology of the area. Eh values are mostly positive (205–398 mV), which indicates oxidising conditions throughout the study area consistent with the influence of AMD. The oxidising conditions, along with the generally low pH, hinder the microbial sulphate reduction, resulting in Fe oxidation. This is a process by which *Acidithiobacillus ferrooxidans* bacteria convert ferrous iron into ferric iron under acidic and oxidising conditions. (Yi et al. 2023). This can influence metal mobility and speciation as ferric iron is the building block for the formation of $Fe(OH)_3$, which typically gives affected water an orange colour referred to as 'yellow-boy'; thereby resulting in reduced DO in the affected water (Zwahlen et al. 2023; Malatji et al 2025; Naghoum et al. 2025). EC values were within acceptable limits (South African Bureau of Standards 2022) at all sampling points except for A4. The lower EC values between B1 and A3 (< 1,500) are below the regulatory limits (South African Bureau of Standards 2022), indicating normal ionic load. However, EC peaks at A4 (> 1,500), indicating a localised ionic overload beyond regulatory limits; higher EC results in osmotic stress in aquatic organisms (Cañedo-Argüelles 2013). Further downstream at A5, dilution and attenuation processes decrease the EC due to the channel entering the river system. In terms of anions, sulphate concentrations exceeded the South African Bureau of Standards 2022 at most sites, confirming the influence of AMD. Relatively lower sulphate concentrations observed at A3 and A4 reflect dilution effects at these points (Miao et al. 2012). In contrast, other anions, such as chloride (Cl^-) and nitrate (NO_3^-), were within standards across all sampling points except for a NO_3 exceedance in A5, which can be potentially traced to anthropogenic sources such as agriculture conducted in the area.

Table 4 In situ physico-chemical parameters and major anions measurements (South African Bureau of Standards 2022)

	pH	Eh (mV)	EC (µS/cm)	DO (mg/L)	SO_4 (mg/L)	Cl (mg/L)	NO_3 (mg/L)
B1	5.0	296.6	1,274	6.5	417	6.40	< 0.194
A1	4.1	350.4	1,119	4.8	415	8.72	< 0.194
A2	4.1	344.7	985	8.1	413	12.5	< 0.194
A3	3.2	398.7	345	5.4	123	11.8	0.212
A4	4.9	318.7	1,772	8.8	108	13.4	< 0.194
A5	7.3	205.1	445	7.2	400	7.53	3.43
South African Bureau of Standards 2022	> 5.0 to < 9.7		< 1,500		< 250	< 250	< 50

Fe concentrations exceeded drinking water standards (< 0.3 mg/L) from B1 to A2, with extremely elevated levels at B1 (45.7 mg/L). This, combined with low pH and elevated sulphate, indicates substantial AMD influence. This is likely due to iron oxidation, a process by which ferrous iron is converted into ferric iron under acidic and oxidising conditions, catalysed by acidophilic bacteria. Ferric iron is further hydrolysed to $Fe(OH)_3$, which results in low DO in aquatic environments (Zwahlen et al. 2023; Malatji et al 2025; Naghoum et al. 2025). Concentrations decline downstream, likely due to dilution and potential precipitation processes such as the dissolution of carbonate minerals, which improves water quality by adding alkalinity. Ca followed a similar trend to Fe, with elevated concentrations near the AMD channel. Ca can contribute to water hardness and may combine with sulphate to form gypsum at varied pH levels (acidic–alkaline), though no gypsum was detected in mineralogical analyses (Zinck & Aubé 2010; Rose 2004; Singh et al. 2005). Despite the presence of Ca and SO_4, the non-detection of gypsum can be traced to the study being conducted during the wet season, which results in run-off from the building blocks of the gypsum (Ca and SO_4). Mg and Cr were generally within acceptable standards, except for a single Mg exceedance at A2. Mn exceeded standards

(< 0.1 mg/L) at all sites, reflecting persistent mobility under the prevailing acidic conditions. According to Doyle & Figueroa (2024), one of the precipitation products of Mn is MnO_2, which occurs as a result of the oxidation of Mn^{2+}. Under the prevailing conditions (acidic and oxidising environments due to AMD), the oxidation of Mn^{2+} to insoluble MnO_2 is very slow. Furthermore, the measured pH values (< 5.1) favour its continued solubility, as Mn precipitation requires a higher pH > 9 (Yang et al 2023; Li et al. 2019; Queiroz et al 2020). Overall, elevated pH/near neutral to basic conditions promotes metal adsorption and precipitation in sediments, while acidic conditions disrupt metal–sediment binding, thereby resulting in mobilisation (Zhang et al. 2014).

Toxicity in aquatic organisms is evaluated using median effective concentrations (EC_{50}) and median lethal concentrations (LC_{50}), which measure how much of a substance is needed to cause an effect or death in 50% of a test group (Brunton et al. 2023; Du & Li 2025). With Fe and Mn being the most problematic in the study area, comparing their concentrations against their toxicity thresholds (EC50 and LC50) would provide insight into the level of exposure. Although Fe and Mn concentrations routinely exceed the South African Bureau of Standards 2022 limit, their potential exposure to aquatic organisms is of greater concern. Fe concentrations across the channel (4.67–45.7 mg/L) are much higher than the acute 48-hour LC_{50} for *Daphnia* species (6.47mg/L), measured by Ghazy et al. (2024), thereby causing toxicity. Mn concentrations (2.71–15.2 mg/L) are also higher than the 48-hour EC_{50} early life-stage fish (0.8–2.1 mg/L), resulting in toxicity (Manganese Consortium 2025). Prolonged exposure to such conditions may result in negative changes in community structure and populations of some aquatic organisms.

Table 5 Concentration of major cations (South African Bureau of Standards 2022)

	Fe (mg/L)	Ca (mg/L)	Mg mg/L)	Mn (mg/L)	Cr (mg/L)
B1	45.7	57.8	23.4	6.48	0.019
A1	4.67	77.9	26.6	15.2	< 0.003
A2	3.99	79.8	34.1	14.3	< 0.003
A3	< 0.004	29.6	16.0	4.10	< 0.003
A4	0.062	20.3	15.7	2.71	< 0.003
A5	< 0.004	159	26.5	14.2	< 0.003
South African Bureau of Standards 2022	< 0.3			< 0.1	< 0.2

The sediments in the study area are mostly siliceous, reflecting a dominant quartz composition that has a poor metal adsorption capacity. The water in the area is characterised by a combination of low pH, high sulphate and elevated metals, resulting in acidic and oxidising conditions (indicative of active AMD contamination). Under such conditions, metals such as Fe and Mn are subjected to an oxidation and hydrolysis process, resulting in their solubility rather than precipitation; this makes them mobile and poses a risk to downstream water quality (Björnerås 2019). Furthermore, the oxidation of Mn^{2+} to a more insoluble MnO_2 is slow in the study area, which results in its mobility. Dilution downstream and precipitation partially mitigate these effects, but persistent acidity and metal mobility suggest ongoing environmental stress in the AMD-affected channel. This highlights that the prevailing water chemistry and sediment composition strongly influence the solubility and mobility of Fe and Mn, resulting in potential ecological risk in the Boesmanspruit catchment.

3.3 Metal speciation

Figure 4 presents the fractionation of Fe, Ca, Mn, Mg and Cr across the sequential extraction procedure, illustrating their distribution among the exchangeable (F1), reducible (F2), oxidisable (F3) and residual (F4) fractions.

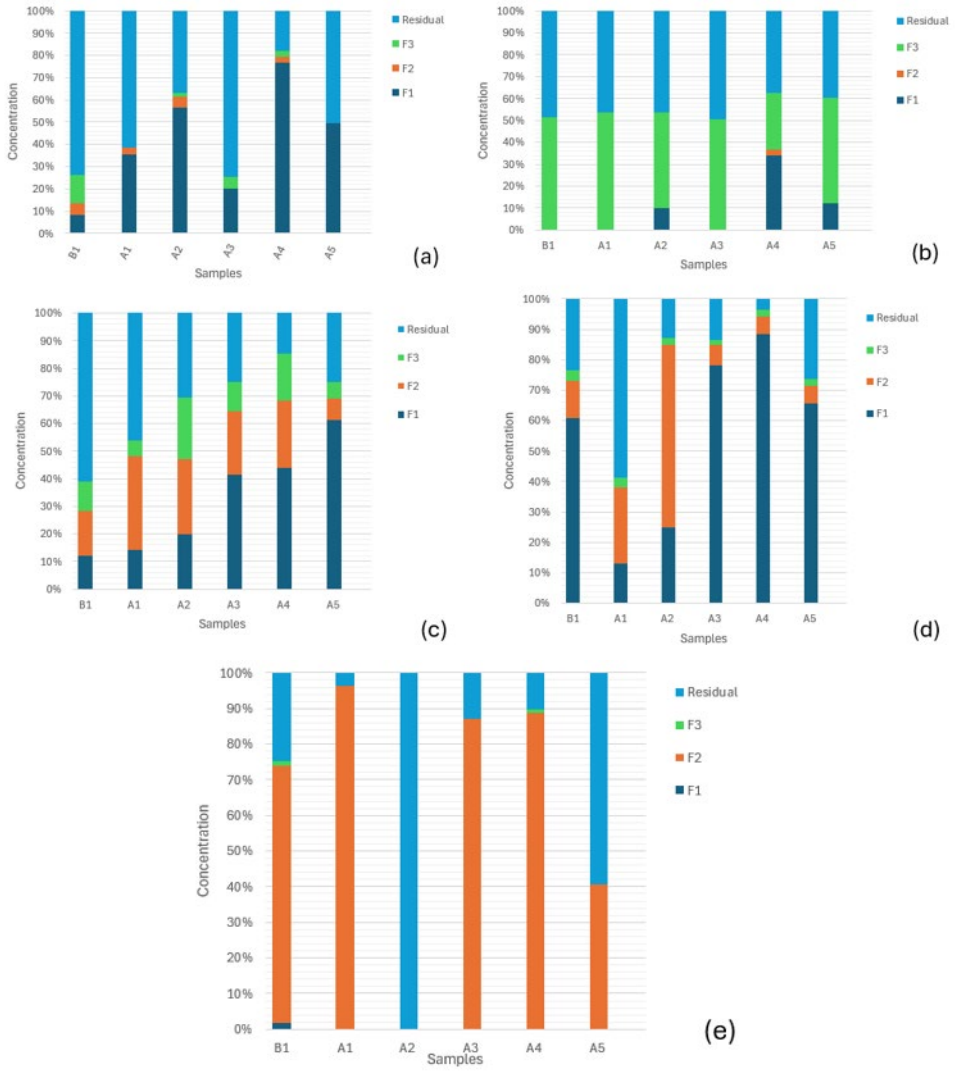

Figure 4 Metal distribution among the different fractions: (a) Calcium; (b) Magnesium; (c) Iron; (d) Manganese; (e) Total chromium

The results provide insight into the mobility, bioavailability and potential environmental risk of these metals in sediments from the study area. It was observed that:

- Calcium and Magnesium: 52% of Ca was associated with the residual fraction, while 42% was associated with the F1 fraction. This presents a duality in which most of the Ca was strongly bound to the sediments and immobile, especially at points B1 and A5, where the pH is high and Eh is positive. Almost half of the Ca was bound to sediment or soil particles and can be released through ion exchange processes or slight decreases in pH, making them highly mobile under the prevailing conditions. This was observed between A1 and A4, where pH levels dropped. In contrast, 45% Mg was associated mainly with the F3 and 44% with the residual fraction. The high association with the F3 fraction reflects complexation with sulphide minerals and organic matter. A lesser amount, 11%, is associated with the F1 fraction, which limits their mobility under the current environmental conditions (Benamer 2014; Singh et al. 2005).
- Iron: it was expected that Fe would be mostly associated with the F1 fraction, but about 33.5% of Fe was associated with the residual fraction, while a lesser 31.8% was associated with the exchangeable fraction (F1). The likeliest explanation for this is the high iron loading observed between B1 and A1, with iron concentration recorded at 45.7 and 4.67 mg/L, respectively. Furthermore, due to the wet season, the hydrolysis of Fe and the deposition of amorphous $Fe(OH)_3$

along the channel can also explain this. Lesser portions were associated with F2 and 3. The presence of Fe in F1, where it is weakly bound to carbonate minerals, makes it readily releasable under moderately acidic conditions (Moyo et al 2015). In F2, Fe is associated with iron and manganese oxides and can become available under reducing conditions, indicating a risk of environmental toxicity. Overall, Fe exhibited high potential mobility under the current environmental conditions (Singh et al. 2005; Tessier et al. 1979).

- Manganese: Mn was expected to be associated with the F2 fraction, but it was mostly associated with the exchangeable fraction (F1, > 65%). The likeliest explanation for this is that the study area is mostly composed of quartz, which has a low surface adsorption area for metals and provides no adsorption surfaces for Mn. The association of Mn with the F2 fraction suggests high mobility under the current environmental conditions. Due to the low pH and Eh, the channel is mostly acidic and oxidising. Under such conditions, the oxidation of Mn to an insoluble product, MnO_2, is slow, resulting in dissolved Mn in the channel. The association of Mn with this fraction results in Mn being easily released under slightly acidic conditions, posing a risk to aquatic ecosystems (Benamer 2014; Singh et al. 2005).
- Chromium: Cr was primarily associated with the reducible fraction (F2), which is associated with Fe–Mn oxides. Based on the water chemistry data, Cr concentrations decreased from 0.019 mg/L at B1 to below the detection limit at downstream points. This is indicative of precipitation due to the oxidation of Fe, which coprecipitates with Cr under oxidising conditions. The oxidation and hydrolysis of Fe form oxyhydroxides that provide an adsorption surface for Cr. According to Zhao et al. (2017), Cr exists as 2 oxidation states, namely CrIII and CrVI, in natural waters, and prevailing pH and redox conditions govern the oxidation states. CrIII is mobile at low pH and has an affinity for Fe hydroxides, resulting in complexation, whereas CrVI is highly soluble across a variety of pH ranges. Due to the presence of Fe phases, CrVI is likely to be reduced to CrIII to form surface complexes.

Overall, the mobility of metals in the study area is largely governed by the interaction of the prevailing geochemical conditions; in this case, acidic and oxidising conditions associated with AMD, as well as the mineralogical composition of the sediments. According to Manyatshe et al. (2017), metals associated with the exchangeable fraction are the most soluble and readily available to the environment, followed by those associated with the reducible, then the oxidisable and, finally, the residual fraction. This order reflects decreasing potential for environmental release and biological uptake. In the studied sediment samples from the study area, the observed general trend in mobility is Mn > Fe > Ca > Cr > Mg.

Quantitative comparison of the distribution of the metals, as well as the rank of their mobility and environmental risk across the fractions, is presented Table 6. It was observed that Mn is mostly associated with the exchangeable fraction, posing the highest environmental risk and making it highly mobile in the area. Fe is associated with both the exchangeable and reducible fractions, giving it moderate mobility. Ca is mainly associated with the residual fraction but can become available due to its significant association with the exchangeable fraction (42%) if conditions permit. Cr is largely associated with the reducible fraction, remaining stable under oxidising conditions; however, it can become mobile under reducing conditions. Mg is mostly associated with F3 and the residual fractions, remaining stable and immobile.

Table 6 Quantitative comparison of metals across fractions

Metal	F1	F2	F3	Residual	Mobility and environmental risk
Mn	> 65%	Minor	Trace	35%	High (immediate risk)
Fe	31.8%	Minor	Minor	33.5%	Moderate (dynamic risk)
Ca	42%	Trace	Trace	52%	Conditional (buffer phase)
Cr	0%	100%	Trace	Trace	Potential mobility (dependent Fe phases)
Mg	11%	Trace	45%	44%	Immobile (stable)

An assessment of the ranking of mobility revealed variable mobility across the sampling points. This is likely due to the interaction between variable site-specific geochemical conditions and variable mineralogical composition of the sediments across the study area (see Figure 5).

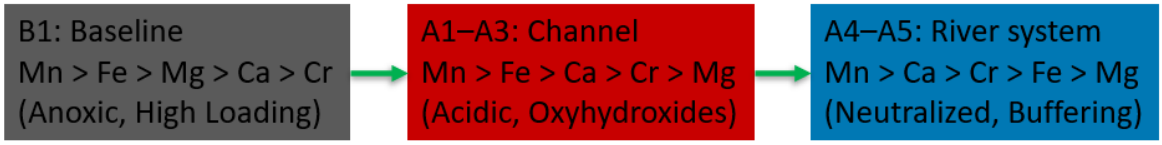

Figure 5 Ranking of metal mobility across sampling points

3.4 Post-extraction elemental and mineralogical composition

3.4.1 Post-extraction elemental composition

The major elemental composition of the sediments after the extraction procedure was determined using XRF, with results expressed as percentages of their respective oxides (Table 7). The analysis showed that SiO_2 was the most dominant oxide, ranging from 82.77 to 92.76%, followed by Al_2O_3, which varied between 3.47 and 9.51% across all samples. The concentration for K_2O ranged between 0.618 and 2.38%, followed by Fe_2O_3, ranging from 0.542 to 1.28%. Other oxides, including TiO_2, MnO, MgO, CaO, Na_2O, P_2O_5, and Cr_2O_3, were present at much lower concentrations, each not exceeding 0.1%.

Table 7 Post-extraction elemental composition

	A1	A2	A3	A4	A5	B1
SiO_2	83.65	86.64	92.24	82.77	86.35	92.76
TiO_2	0.467	0.472	0.497	0.755	0.466	0.259
Al_2O_3	8.61	8.04	4.40	9.51	7.79	3.47
Fe_2O_3 (t)	0.545	0.686	0.542	1.00	0.644	1.28
MnO	0.008	0.006	0.008	0.015	0.007	0.005
MgO	< 0.02	< 0.02	< 0.02	< 0.02	< 0.02	< 0.02
CaO	0.035	0.019	0.029	0.037	0.023	0.047
Na_2O	0.11	0.08	0.06	0.21	0.17	0.05
K_2O	1.69	1.17	1.11	2.38	1.87	0.618
P_2O_5	0.02	0.02	0.01	0.03	0.02	0.02
Cr_2O_3	0.012	0.009	0.015	0.014	0.015	0.015
LOI	5.19	3.24	1.26	3.19	2.90	2.03
Total	100.35	100.40	100.14	99.87	100.20	100.53
H_2O^-	1.12	1.07	0.40	1.00	0.98	0.56

Comparison of the baseline and post-extraction elemental composition indicates successful extraction of mobile phases, leaving behind pure SiO_2 hence it seems relatively enriched in the residual sediments. According to Wang et al. (2023), quartz has a low cation exchange capacity and limited surface reactivity, reducing its capacity to adsorb metals compared to clay minerals and iron oxides, hence it is unreactive in the study area. The successful extraction has also resulted in a massive depletion of mobile phases such as Fe and Cr, hence their relative low concentration in post extraction results. The extraction confirms that CrIII was bound to reducible fraction, by adsorbing to Fe oxyhydroxides to form near surface complexes. Mn is highly mobile; this is confirmed by its relative disappearance across the board in the extraction residue. Secondary sodium/potassium increases indicate trace reagent residues.

3.4.2 Post-extraction mineralogical composition

The mineralogical composition of sediments collected after the extraction procedure is illustrated in Table 8. Quartz was identified as the dominant mineral, accounting for 71–80% of the sediment across all samples. The second-most abundant mineral was wooldridgeite, at concentrations ranging from 20–30% across all samples.

Table 8 Post-extraction mineralogical composition

Sample ID	Wooldridgeite	Quartz	Plagioclase
B1	20	80	–
A1	29	71	29
A2	24	76	–
A3	20	80	–
A4	30	70	–
A5	21	79	–

Comparison of the baseline and post-extraction mineralogy indicates that the sequential extraction procedure dissolved and transformed existing minerals into new minerals. The fate of quartz is discussed in section 3.4.1 but in summary, quartz was not dissolved or transformed but rather washed to its pure form. Clinochore and K-feldspar were completely dissolved as they don't appear in post-extraction residual sediments. This is likely due to the extraction chemicals used during the procedure destroying them. The appearance of wooldridgeite is completely artificial and likely due to laboratory conditions (Cooper et al. 2000). The emergence of plagioclase represents a structural recrystallisation of unreacted calcium/sodium fractions due to the breakdown of baseline clinochlore; a common phenomenon during dissolution-precipitation processes (Konrad-Schmolke et al. 2018; Cuadros 2025).

4 Conclusion

This study demonstrates that the prevailing conditions, namely, shifts in pH and redox conditions [due to acid mine drainage (AMD)], as well as the composition of the sediments (quartz-dominated), govern the retention and release of metals in the area. In oxidising conditions, AMD-released Fe undergoes oxidation and hydrolysis, forming amorphous Fe oxyhydroxides. These provide highly reactive surfaces for Cr to adsorb; this reduces its concentrations and promotes its association with the reducible fraction. Even though such processes limit the mobility of Cr, its retention in the sediments is temporary. If conditions permit (reducing conditions), the Cr may be released back into the water column. In terms of Mn, its association with the exchangeable fraction (> 65%) indicates that ion exchange processes or low pH may remobilise it as it is weakly bound to sediments. The elevated Mn concentration throughout the study area reflects this and is a result of the slow oxidation of Mn to a more insoluble form under acidic conditions. Overall, these findings show that the sediments are not only a sink for metals but also a potential long-term secondary source of contamination under changing physico-chemical conditions.

From an environmental management perspective, passive treatment systems such as the reducing and alkalinity producing system (RAPS) are suggested to treat the AMD. This is due to their cost effectiveness as well as the chemistry and flow of the AMD in the area. But they would need to be optimised to include a manganese bed to specifically treat Mn, as it requires a higher pH to precipitate.

The study faces limitations due to the operational nature of the SM&T sequential extraction procedure, potential oxidation of samples during processing and misleading results due to the high-flow wet season. Such limitations risk artificially shifting metal fractions and misrepresenting the stable mineral phases that are expected to alter during the low-flow dry season.

Acknowledgement

The authors thank the Council for Geoscience and the Department of Mineral and Petroleum Resources for funding this research.

References

Aswal, RS, Prasad, M, Patel, NKA, Srivastav, L, Egbueri, JC, Kumar, G & Ramola, RC 2023, 'Occurrences, sources and health hazard estimation of potentially toxic elements in the groundwater of Garhwal Himalaya, India', *Scientific Reports,* vol. 13, no. 13069, https://doi.org/10.1038/s41598-023-40266-7

Benamer, MA 2014, *Chemical Speciation and Spatial Distribution of Heavy Metals and Their Adsorption Onto Sediments of the Berg River, South Africa*, PhD thesis, University of Cape Town, Cape Town.

Björnerås, C 2019, *Drivers of Increasing Iron Concentrations in Freshwaters*, PhD thesis, Lund University, Lund.

Brime, C 1985, 'The accuracy of X-ray diffraction method for determining mineral mixtures', *Mineralogical Mag*, vol. 49, pp. 531–538.

Brunton, LL, Knollmann, BC, & Hilal-Dandan, R (Ed) 2023, *Goodman & Gilman's: The Pharmacological Basis of Therapeutics*, 14th edn, McGraw Hill, Ohio.

Cañedo-Argüelles, M, Kefford, BJ, Piscart, C, Prat, N, Schäfer, R & Schulz, 2013, 'C Salinisation of rivers: An urgent ecological issue', *Environmental Pollution*, vol. 173, pp. 157–167, https://doi.org/10.1016/j.envpol.2012.10.011

Chidzungu, T 2019, *Perspectives on the Role of Social Impact Assessments in Solving Acid Mine Drainage Imposed Socio-Economic Impacts in Post-Mining Communities: A study of Carolina Catchment Area X11B in Mpumalanga, South Africa*, MSc thesis, University of the Witwatersrand, Johannesburg.

Cloet, HCC 2022, *The Estimation of Uncertainty of Measurement by X-ray Fluorescence Spectrometry,* MSc thesis, University of Johannesburg, Johannesburg.

Cooper MA, Hawthorne FC & Cerny P 2000 'Refinement of the crystal structure of wooldridgeite, $Na_2CaCu^{2+}{}_2(P_2O_7)_2(H_2O)_{10}$, a novel copper pyrophosphate mineral', *Canadian Mineralogist,* vol. 37, pp. 73–81.

CSIR 2013, *Characterising the Risk of Human Exposure and Health Impacts from Acid Mine Drainage in South Africa Deliverable for Output VII–"Final Project Report"*, Council for Scientific and Industrial Research, Pretoria.

Cuadros, J 2025, 'Clay on Mars', in F Bergaya & P Yuan (eds), *Developments in Clay Science*, vol. 12, Elsevier, Amsterdam.

Doyle, S & Figueroa, L 2024, 'Electrolytic Manganese Removal from Acid Rock Drainage' in B Kleinmann, J Skousen, C Wolkersdorfer (eds), *Proceedings of the 15th International Mine Water Association Congress*, International Mine Water Association, Virginia, pp. 151–156.

Du, Z & Li, J 2025 'Clarifying the misuse of EC50, IC50, and LC50 in cytotoxicity study of water disinfection byproducts: A critical analysis and perspective', *Hygiene and Environmental Health Advances.*

Dube, M, Ramasenya, K & van Zweel, N 2019, 'The use of passive treatment systems to remediate AMD from abandoned coal mines, Emalahleni, South Africa — column experiments', in E Khayrulina, C Wolkersdorfer, S Polyakova & A Bogush (eds), *Mine Water — Technological and Ecological Challenges*, pp. 167–175.

Dzhangi, T & Atangana, E, 2024, 'Evaluation of the impact of coal mining on surface water in the Boesmanspruit, Mpumalanga, South Africa', *Environmental Earth Sciences*, vol 83, pp. 1–21.

Favas, P, Pratas, J, Gomes, M & Cala, V 2011, 'Selective Chemical Extraction of Heavy Metals in Tailings and Soils Contaminated by Mining Activity: Environmental Implications', *Journal of Geochemical Exploration*, vol. 111, pp. 160–171.

Galán, E, Gómez-Ariza, JL, González, I, Fernández-Caliani, J, Morales, E & Giráldez, I 2003, 'Heavy metal partitioning in river sediments severely polluted by acid mine drainage in the Iberian Pyrite Belt', *Applied Geochemistry*, vol. 18, pp. 409–421.

Geldenhuis, S & Bell, FG 1998, 'Acid mine drainage at a coal mine in the eastern Transvaal, South Africa', *Environmental Geology,* vol. 34, pp. 234–242.

Greenshields, HD 1986, 'Eastern Transvaal Coalfield', in CR Anhaeusser & S Maske (eds), *Mineral Deposits of Southern Africa, vol. II, South African Journal of Geology*, pp. 1995–2010.

Hancox, J & Götz, A 2014, 'South Africa's coalfields — A 2014 perspective', *International Journal of Coal Geology*, vol. 132, pp. 170–254.

Jennings, SR, Neuman, DR & Blicker, PS 2008, *Acid Mine Drainage and Effects on Fish Health and Ecology: A Review*, Reclamation Research Group Publication, Bozeman.

Konrad-Schmolke M, Halama R, Wirth R, Thomen A, Klitscher N, Morales L, Schreiber A & Wilke FDH 2018, Mineral dissolution and reprecipitation mediated by an amorphous phase, *Nature Communications*, vol. 24, no. 9.

Korfali, S & Davies, B 2004, 'Speciation of metals in sediment and water in a river underlain by limestone: Role of carbonate species for purification capacity of rivers' *Advances in Environmental Research*, vol. 8, pp. 599–612.

Landner, L & Reuther, R 2005, 'Speciation, mobility and bioavailability of metals in the environment', *Metals in Society and in the Environment*, vol 8. https://doi.org/10.1007/1-4020-2742-7_6

Li, Y, Xu, Z, Ma, H, Hursthouse, A 2019, 'Removal of manganese(II) from acid mine wastewater: a review of the challenges and opportunities with special emphasis on Mn-oxidizing bacteria and microalgae', *Water*, vol. 11, no. 2493, https://doi.org/10.3390/w11122493

Lloyd, PJ 2013, *Coal Mining and the Environment*, Energy Research Institute, University of Cape Town, Cape Town.

Ghazy, M, Habashy, M & Nassif, G 2024, 'The acute toxic impact of iron (Fe) and lead (Pb) individually and their mixture on Daphnia magna (Straus, 1820)', *Egyptian Journal of Aquatic Biology & Fisheries*, vol. 28, no. 2, pp. 675–683.

Malatji, M, Fosso-Kankeu, E & Mamba, B 2025, 'A review of the reducing and alkalinity-producing system (RAPS) for acid mine drainage neutralization', in E Fosso-Kankeu, V Masindi, J Maree & B Mamba (eds), *Customized Technologies for Sustainable Management of Industrial Wastewater: A Circular Economy Approach*, Scrivener Publishing LLC, Beverly, pp. 3–38.

Manganese Consortium. (2025). *Safety Data Sheet: Manganese Dinitrate; Manganese (2+) Dinitrate*, Paris. Retrieved from www.reach-manganese.org

Manyatshe, A, Fosso-Kankeu, E, Berg, D, Lemmer, N, Waanders, F & Tutu, H 2017, 'Metal retention potential of sediment and water quality in the Mooi River, South Africa', *Desalination and Water Treatment*, vol. 66, pp. 346–357.

Maphanga, T, Chidi, BS, Phungela, T, Gqomfa, B, Madonsela, B, Malakane, K, Lekata, S & Shale, K 2024, 'The interplay between temporal and seasonal distribution of heavy metals and physiochemical properties in Kaap River', *International journal of Environmental Science and Technology*, vol. 21, no. 10.

Mashalane, TB, Novhe, NO, Yibas, B, Coetzee, H & Wolkersdorfer, C 2018, 'Metal removal from mine water using passive treatment technologies (anaerobic and aerobic) in the Ermelo Coalfields, Mpumalanga', *South Africa: Risk to Opportunity 2018: Proceedings of the 11th International Mine Water Association*, IMWA, Pretoria, pp. 146–150.

McCarthy, TS 2011, 'The impact of acid mine drainage in South Africa', *South African Journal of Science*, vol. 107, no. 5/6.

McCarthy, TS, Humphries, MS 2013 'Contamination of the water supply to the town of Carolina, Mpumalanga', *South African Journal of Science*, vol. 109, no. 9/10, pp. 1–10.

Mello, T, Malatji, M, Phahlane, T, Safi, M, Coetzee, H & Phakula, D 2024, *Mine and Environmental Water Management Programme: Passive Treatment of Polluted Mine Water in Carolina, Mpumalanga,* (Report number: 2023-0089), Council for Geoscience, Pretoria.

Miao, Z, Brusseau, M, Carroll, K, Carreón-Diazconti, C & Johnson, B 2012, 'Sulfate reduction in groundwater: characterisation and applications for remediation', *Environmental Geochemistry and Health*, vol. 34, no. 4, pp. 39–50.

Miller, JR, Gannon, JP & Corcoran, K 2019, 'Concentrations, mobility, and potential ecological risks of selected metals within compost amended, reclaimed coal mine soils, tropical South Sumatra, Indonesia', *AIMS Environmental Science,* vol. 6, no. 4, pp. 298–325.

Mitra, S, Chakraborty, A, Tareq, A, Emran, T, Nainu, F, Khusro, A, … Simal-Gandara, J 2022, 'Impact of heavy metals on the environment and human health: Novel therapeutic insights to counter the toxicity', *Journal of King Saud University - Science*.

Miranda, LS, Ayoko, GA, Egodawatta, P, & Goonetilleke, A 2022, 'Adsorption-desorption behaviour of heavy metals in aquatic environments: Influence of sediment, water and metal ionic properties', *Journal of Hazardous Materials*, vol. 421.

Moyo, S, McCrindle, RI, Mokgalaka, N & Myburgh, J 2015, 'Heavy metal partitioning in sediments from rivers flowing through coal fields in Mpumalanga, South Africa', *Clean - Soil, Air, Water*, vol. 43, no. 6, pp. 892–900.

Munnik, V 2010, '*The Social and Environmental Consequences of Coal Mining in South Africa: a case study*' https://static1.squarespace.com/static/5a7859a10abd0477ecb31301/t/5c5d88fbe5ef0151ead5a97/1549633797101/2010Jan__Coal_in_SA_Social_and_Env_Impacts.pdf

Naghoum, I, Edahbi, M, Melián, JAH, Doña Rodriguez, JM, Durães, N, Pascual, BA & Salmoun, F 2025, 'Passive treatment of acid mine drainage effluents using constructed wetlands: case of an abandoned iron mine, Morocco', *Water*, vol. 17, no. 687, https://doi.org/10.3390/w17050687

Namieśnik, J & Rabajczyk, A 2010, 'The speciation and physico-chemical forms of metals in surface waters and sediments', *Chemical Speciation and Bioavailability*, vol. 22, pp. 1–24.

Nemati, K, Abu Bakar, NK, Abas, R & Sobhanzadeh, E 2011, 'Speciation of heavy metals by modified BCR sequential extraction procedure in different depths of sediments from Sungai Buloh, Selangor, Malaysia', *Journal of Hazardous Materials*, vol. 192, no. 1, pp. 402–410.

Nethavhani, EC 2012, *Seasonal Variations and Trends of Nitrates and Phosphates Concentration Along the Boesmanspruit River in Mpumalanga Province*, MSc thesis, University of Johannesburg, Johannesburg.

Novhe, O, Yibas, B, Coetzee, H, Atanasova, M, Netshitungulwana, R, Modiba, M & Mashalane, T 2016, 'Long-term remediation of acid mine drainage from abandoned coal mine using integrated (anaerobic and aerobic) passive treatment system in South Africa: A pilot study', *Mining Meets Water – Conflicts and Solutions*, vol. 1, pp. 668–675.

Ojonimi, T, Asuke, F, Onimisi, M & Onuh, C 2019, 'Acid Mine Drainage (AMD): an environmental concern generated by coal mining', *Journal of Degraded and Mining Lands Management,* vol. 6, on. 4, pp. 1875–1881.

Pope, J, Weber, P, Mackenzie, A, Newman, N & Rait, R 2010, 'Correlation of acid base accounting characteristics with the Geology of commonly mined coal measures, West Coast and Southland, New Zealand', *New Zealand Journal of Geology and Geophysics*, vol. 53, no. 2–3, pp. 153–166, https://doi.org/10.1080/00288306.2010.498404

Rose, A 2004, 'Vertical flow systems - effects of time and acidity relations', *Journal American Society of Mining and Reclamation*, pp. 1595–1616.

Queiroz, HM, Ying, SC, Abernathy, M, Barcellos, D, Gabriel, FA, Otero, XL, … Ferreira, TO 2020, 'Manganese: the overlooked containment in the world's largest mine tailings dam collapse', *Environmental International*, vol. 146, no. 106284, https://doi.org/10.1016/j.envint.2020.106284

Sakala, E, Fourie, F, Gomo, M, Coetzee, H 2017, 'Hydrogeological investigation of Witbank, Ermelo and Highveld Coalfields: Implications for acid mine drainage subsurface transport and attenuation', in C Wolkersdorfer, L Sartz, M Sillanpää & A Häkkinen (eds), *Mine Water & Circular Economy*, vol. I, pp. 564–572.

Shongwe, BN 2018, *The Impact of Coal Mining on the Environment and Community Quality of Life: A Case Study Investigation of the Impacts and Conflicts Associated with Coal Mining in the Mpumalanga Province, South Africa*, MSc thesis, University of Cape Town, Cape Town.

Singh, K, Mohan, D, Singh, VK, & Malik, A 2005, 'Studies on distribution and fractionation of heavy metals in Gomti river sediments—a tributary of the Ganges, India', *Journal of Hydrology*, vol. 312, pp. 1–4. https://doi.org/10.1016/j.jhydrol.2005.01.021

South African Bureau of Standards 2022, '*Draft South African Standard: SANS 241: XXXXX edition 7 – Drinking water quality*', South African Bureau of Standards, Pretoria.

Tessier, A, Campbell, PGC & Bisson, M 1979, 'Sequential Extraction Procedure for the Speciation of Particulate Trace Metals', *Analytical Chemistry*, vol. 51, pp. 844–851, https://doi.org/10.1021/ac50043a017

Tokalioglu, S, Kartal, S & Birol, G 2003, 'Application of a three-stage sequential extraction procedure for the determination of extractable metal contents in highway soils', *Turkish Journal of Chemistry*, vol. 27, pp. 333–346.

Violante, A, Cozzolino, V, Perelomov, L, Caporale, AG, & Pigna, M 2010, 'Mobility and bioavailability of heavy metals and metalloids in soil environments', *Journal of Soil Science and Plant Nutrition*, vol. 10, no. 3, pp. 268–292.

Wang, T, Cao, W, Wang, Y, Qu, C, Xu, Y & Li, H 2023, 'Surface modification of quartz sand: A review of its progress and its effect on heavy metal adsorption', *Ecotoxicology and Environmental Safety*, vol. 262, no. 115179.

Yang, F, Li, J, Wang, H, Xiao, X, Bai, R Feng 2023, 'Visible light induces bacteria to produce superoxide for manganese oxidation', *Frontiers of Environmental Science & Engineering*, vol. 17, no. 2, https://doi.org/10.1007/s11783-023-1619-y

Yi, Q, Wu, S, Liu, Y, Chan, T, Lu, Y, Saha, N, Southam, G & Huang, L 2023, 'Mineral weathering of iron ore tailings primed by Acidithiobacillus ferrooxidans and elemental sulfur under contrasting pH conditions', *Science of The Total Environment*, vol. 856, https://doi.org/10.1016/j.scitotenv.2022.159078

Zhang, C, Yu, Z, Zeng, G, Jiang, M, Yang, Z, Cui, F, Zhu, M, Shen, L, Hu, L 2014, 'Effects of sediment geochemical properties on heavy metal bioavailability' *Environment international*, vol. 73, pp. 270–281.

Zhao, J, Al, T, Chapman, SW, Parker, BL, Mishkin, KR, Cutt, D, Wilkin, RT 2017, 'Determination of Cr(III) solids formed by reduction of Cr(VI) in a contaminated fractured bedrock aquifer: evidence for natural attenuation of Cr(VI)', *Chemical Geology*, vol. 10, no. 474, pp. 1–8.

Zhou, Q, Yang, N, Li, Y, Ren, B, Ding, X, Bian, H, & Yao, X 2020, 'Total concentrations and sources of heavy metal pollution in global river and lake water bodies from 1972 to 2017', *Global Ecology and Conservation*, vol. 22.

Zinck, J, & Aubé, B 2010, *Overcoming Active Treatment Challenges*, CANMET-Mining and Mineral Science Laboratories, Natural Resources Canada.

Zwahlen, C, Rehn, A, Aiglsperger, T, Dold, B 2023, 'Geochemical and mineralogical aspects of acid mine drainage associated with 100 years of coal mining in the arctic, Svalbard (78◦N)', *Journal of Geochemical Exploration*, vol. 252, no. 107266, https://doi.org/10.1016/j.gexplo.2023.107266